

Anna Yesypenko and Per-Gunnar Martinsson
 Oden Institute, University of Texas at Austin

Abstract: The paper describes a sparse direct solver for the linear systems that arise from the discretization of an elliptic PDE on a two dimensional domain. The solver is designed to reduce communication costs and perform well on GPUs; it uses a two-level framework, which is easier to implement and optimize than traditional multi-frontal schemes based on hierarchical nested dissection orderings. The scheme decomposes the domain into thin subdomains, or “slabs”. Within each slab, a local factorization is executed that exploits the geometry of the local domain. A global factorization is then obtained through the LU factorization of a block-tridiagonal reduced coefficient matrix. The solver has complexity $O(N^{5/3})$ for the factorization step, and $O(N^{7/6})$ for each solve once the factorization is completed.

The solver described is compatible with a range of different local discretizations, and numerical experiments demonstrate its performance for regular discretizations of rectangular and curved geometries. The technique becomes particularly efficient when combined with very high-order convergent multi-domain spectral collocation schemes. With this discretization, a Helmholtz problem on a domain of size $1000\lambda \times 1000\lambda$ (for which $N = 100\text{M}$) is solved in 15 minutes to 6 correct digits on a high-powered desktop with GPU acceleration.

1. INTRODUCTION

1.1. **Problem setup.** We present a direct solver for boundary value problem of the form

$$(1) \quad \begin{cases} \mathcal{A}u(x) = f(x), & x \in \Omega, \\ u(x) = g(x), & x \in \partial\Omega, \end{cases}$$

where \mathcal{A} is a second order elliptic differential operator, and Ω is a domain in two dimensions with boundary $\partial\Omega$. The method works for a broad range of constant and variable coefficient differential operators, but is particularly competitive for problems with highly oscillatory solutions that are difficult to pre-condition. For the sake of concreteness, we will focus on the case where \mathcal{A} is a variable coefficient Helmholtz operator

$$(2) \quad \mathcal{A}u(x) = -\Delta u(x) - \kappa^2 b(x)u(x),$$

where κ is a reference (“typical”) wavenumber, and where $b(x)$ is a smooth non-negative function. Upon discretizing (1), one obtains a linear system

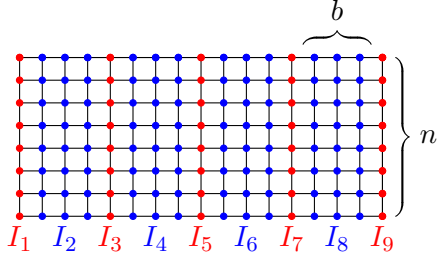
$$(3) \quad \mathbf{A}\mathbf{u} = \mathbf{f},$$

involving a coefficient matrix \mathbf{A} that is typically sparse. Our focus is on efficient algorithms for directly building an invertible factorization of the matrix \mathbf{A} . We specifically consider two different discretization schemes, first a basic finite difference scheme with second order convergence, and then a high (say $p = 20$) order multidomain spectral collocation scheme [32, Ch. 25]. However, the techniques presented can easily be used with other (local) discretization schemes such as finite element methods.

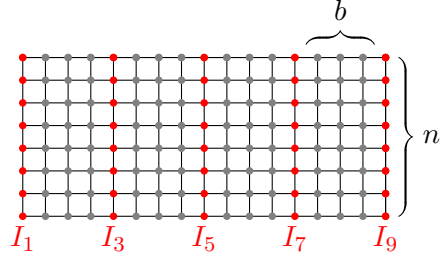
1.2. **Overview of proposed solver.** The solver presented is based on a decomposition of the computational domain into thin “slabs”, as illustrated in Figure 1a. Unlike previously proposed sweeping schemes [16, 18, 38] designed for preconditioning, our objective is to directly

factorize the coefficient matrix, or at least compute a factorization that is sufficiently accurate that it can handle problems involving strong backscattering.

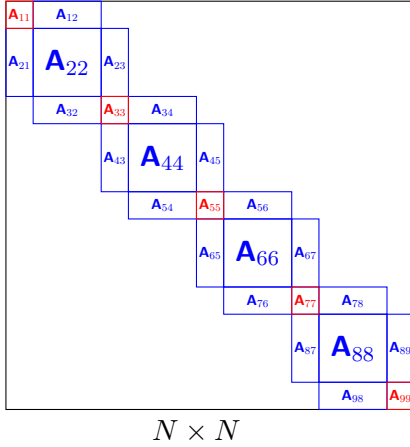
To describe how the solver works, let us consider a simple model problem where the PDE is discretized using a standard five-point finite difference stencil on a uniform grid such as the one shown in Figure 1a. The nodes in the grid are arranged into slabs of width b , and are ordered as shown in Figure 1a, resulting in a coefficient matrix \mathbf{A} with the block diagonal sparsity pattern shown in Figure 1c. The factorization of \mathbf{A} then proceeds through two stages.



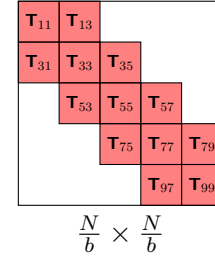
(a) Original grid, partitioned into slabs of width $b + 2$, where $b = 3$.



(b) Reduced grid, after eliminating blue nodes. Only the red nodes are “active”.



(c) Sparsity structure of \mathbf{A} corresponding to the original grid. Each block of \mathbf{A} is sparse.



(d) Sparsity structure of \mathbf{T} corresponding to the reduced grid. Each block of \mathbf{T} is dense.

FIGURE 1. Illustration of the elimination order used in SlabLU.

In the first stage, the nodes that are internal to each slab (identified by the index vectors I_2, I_4, \dots and shown as blue in Figure 1a) are eliminated from the linear system, resulting in the reduced problem shown in Figure 1b, with the associated coefficient matrix shown in Figure 1d. In this elimination step, we exploit that each subdomain is thin, which means that classical sparse direct solvers are particularly fast. To further accelerate this step, we use that the Schur complements that arise upon the elimination of the interior nodes are rank structured. Specifically, they are “HBS/HSS matrices” [24, 40, 41] with *exact* HBS/HSS rank at most $2b$. This allows us to accelerate this reduction step using a recently proposed randomized algorithm for compressing rank structured matrices [27].

The second stage is to factorize the remaining coefficient matrix \mathbf{T} shown in Figure 1d. This matrix is much smaller than the original matrix \mathbf{A} , but its blocks are dense. These blocks are rank structured as well, which could in principle be exploited to attain a linear complexity solver (for the case where the PDE is kept fixed as N increases). However, we have found

that for 2D problems, the dense operations are fast enough that exploiting rank structure for the second step is not worthwhile when $N \leq 10^8$.

A particular advantage of our framework is that it is simple to optimize and accelerate on GPUs, compared to traditional multi-frontal schemes. The numerical results demonstrate compelling speed and memory scaling, when compared to SuperLU [28]. For meshes with 100 million points, the factorization can be computed in 20 minutes on a desktop with an Intel i9-12900k CPU with 16 cores and an RTX 3090 GPU. Once the factorization is available, subsequent solves take about a minute. The numerical results feature timing results on a variety of architectures to demonstrate that the scheme is portable to many hardware settings.

The scheme also interacts very well with high order discretization schemes such as those described in [35] and [32, Ch. 25], which makes it a particularly powerful tool for solving problems with highly oscillatory solutions. The numerical results feature constant and variable coefficient Helmholtz problems on rectangular and curved domains. Using high order discretizations, we are able to discretize the PDE to 10 points per wavelength and accurately resolve solutions on domains of size $1000\lambda \times 1000\lambda$, where λ is the wavelength, to 6 digits of relative accuracy, compared to the true solution of the PDE.

1.3. Context and related work. Methods to solve (3) can be characterized into two groups – direct and iterative. The linear systems involved are typically ill-conditioned, which necessitates the use of pre-conditioners or multigrid solvers. However, preconditioners typically struggle for problems with oscillatory solutions that involve phenomena such as multiple reflections, back-scattering, and waves trapped in cavities [17,18]. Sparse direct methods, which factorize matrix \mathbf{A} exactly, offer a robust means of solving challenging PDEs. Direct solvers are also particularly advantageous in situations involving multiple right-hand sides or low-rank updates to the matrix \mathbf{A} .

The solver we describe in this work is related to multi-frontal LU solvers [13] which often use a hierarchical nested dissection ordering of grid nodes [3,19]. For a 2D grid with N nodes, the resulting techniques have complexity $O(N^{3/2})$ to build and $O(N \log N)$ complexity to solve, which is known to be work optimal among solvers that exploit only sparsity in the system [12,15].

By replacing the nested dissection ordering with a partition into thin slabs, SlabLU improves communication efficiency, and allows the method to better take advantage of hardware accelerators. Nevertheless, its asymptotic flop count is only slightly sub-optimal. Specifically, by choosing $b \sim O(n^{2/3})$, sparsity alone results in complexity $O(N^{5/3})$ for the factorization stage, and $O(N^{7/6})$ for the solve stage, when applied to 2D problems.

The use of rank structured matrix algebra to accelerate sparse direct solvers is inspired by prior work including [2, 10, 20, 23, 36, 42]. A key feature of SlabLU is that unlike prior work, the rank structures that we exploit are *exact*, relying only on the sparsity pattern of the original coefficient matrix (cf. Section 3.2). Importantly, these rank-deficiencies are present in both the non-oscillatory and oscillatory regimes. This makes the randomized compression particularly efficient, achieving very high computational efficiency with no loss of accuracy beyond floating point errors. Another novelty is the usage of a recently developed black box randomized algorithm for compressing rank structured matrices [27] (which in turn draws on insights from [29, 31, 34]) when eliminating the interior nodes in each slab. The use of black-box randomized algorithms makes the solver relatively simple to implement, and easier to port between different local discretization.

SlabLU is also related to Schur complement methods, which are two-level methods based on a non-overlapping domain decomposition with implicit treatment of the interface conditions. The interior of each subdomain is factorized in parallel; the reduced coefficient matrix \mathbf{T} is typically not formed but instead applied matrix-free in an iterative method [9, 37]. These

methods have similar advantages as SlabLU in that they are easy to parallelize. They implicitly solve a reduced system that is better conditioned than the original system, but is often difficult to precondition for oscillatory problems.

1.4. Extensions and limitations. The solver presented is purely algebraic and can be applied to a range of different discretization schemes, including finite element and finite volume methods. In this manuscript, we restrict attention to uniform grids and domains that are either rectangular themselves, or can easily be mapped to a union of rectangles. It is in principle possible to adapt the method to more general discretizations, including ones that involve local refinement. However, some of the accelerations (e.g. batched linear algebra) would in this case lose efficiency to some degree.

While we in this manuscript restrict attention to the two dimensional case, the method is designed to handle three dimensional problems as well. All ideas presented carry over directly, but additional complications do arise. The key challenge is that in three dimensions, it is no longer feasible to use dense linear algebra when factorizing the block tridiagonal reduced coefficient matrix \mathbf{T} . Instead, rank structure must be exploited in both stages of the algorithm, and rank deficiencies will no longer be exact. However, the 3D version of SlabLU is also very easy to parallelize, and the idea of using randomized compression combined with efficient sparse direct solvers to eliminate the nodes interior to each slab still applies, cf. Section 7.

2. DISCRETIZATION AND NODE ORDERING

We introduce two different discretization techniques for (1). The first is simply the standard second order convergent five point finite difference stencil. Since this discretization is very well known, it allows us to describe how the solver works without the need to introduce cumbersome background material. To demonstrate that the solver works for a broader class of discretization schemes, the numerical experiments reported in Section 6 also include results that rely on the high order convergent *Hierarchical Poincaré-Steklov (HPS)* scheme, which we briefly describe in Section 2.3.

2.1. A model problem based on the five point stencil. For purposes of describing the factorization scheme, let us introduce a very simple discretization of the boundary value problem (1). We work with a rectangular domain $\Omega = [0, L_1] \times [0, L_2]$ and the second order linear elliptic operator \mathcal{A} defined by (2). We assume that $L_1 \geq L_2$, and that $L_1 = hn_1$ and $L_2 = hn_2$ for some grid spacing h and some positive integers n_1 and n_2 . We then discretize \mathcal{A} with a standard second-order finite difference scheme, to obtain the linear system

$$(4) \quad \frac{1}{h^2}(\mathbf{u}(n_w) + \mathbf{u}(n_e) + \mathbf{u}(n_n) + \mathbf{u}(n_s) - 4\mathbf{u}(n)) - \kappa^2 \mathbf{b}(n)\mathbf{u}(n) = \mathbf{f}(n).$$

The vector \mathbf{f} holds values of the body load at the discretization nodes, and the vector u holds approximations to the solution u . See Figure 2 for a visualization of the 5 point stencil. We write the system (4) compactly as $\mathbf{A}\mathbf{u} = \mathbf{f}$.

2.2. Clustering of the nodes. We next subdivide the computational domain into thin “slabs”, as shown in Figure 1a. We let b denote the number of grid points in each slab ($b = 4$ in Figure 1a), and then introduce index vectors I_1, I_2, I_3, \dots that keep track of which slabs each grid point belongs to. The odd numbered index vectors I_1, I_3, I_5, \dots indicate nodes on the interfaces between slabs (red in Figure 1a), while the even numbered ones indicate nodes that are interior to each slab (blue in Figure 1a). With this ordering of the grid points, the stiffness matrix associated with the discretization (4) has the sparsity pattern shown in Figure 1c.

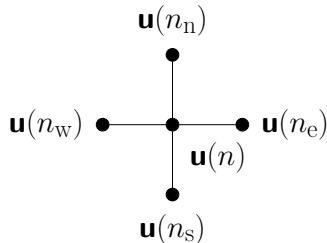


FIGURE 2. Five point stencil in 2D.

2.3. High order discretizations. To accurately resolve oscillatory wave phenomena, we rely on a high order accurate multi-domain spectral collocation discretization known as the Hierarchical Poincaré-Steklov scheme (HPS). This discretization scheme is designed to allow for high choices of the local discretization order p without degrading the performance of direct solvers.

In HPS, the computational domain is subdivided into small rectangles, and a $p \times p$ tensor product grid of Chebyshev nodes is placed on each rectangle, cf. Figure 3. The vector of unknowns \mathbf{u} simply holds approximations to the solution u at the discretization nodes. We then discretize (1) through collocation of the spectral differentiation operator for each internal node. For the nodes on cell boundaries, we enforce continuity of the normal derivatives, again through spectral differentiation.

To improve efficiency when HPS is combined with sparse direct solvers, we "eliminate" the dense interactions of nodes interior to each subdomain through a static condensation step. In SlabLU, this elimination step is accelerated using GPUs with batched linear algebra, which is very efficient for p as high as 42 [43].

The static condensation step leaves us with a reduced linear system that involves the approximately $n_1 n_2 / p$ points that sit on the edges between cells. We denote the reduced stiffness matrix by $\tilde{\mathbf{A}}$, and the reduced load vector by $\tilde{\mathbf{f}}$, cf. Figure 3, to obtain the equivalent system

$$(5) \quad \tilde{\mathbf{A}}\tilde{\mathbf{u}} = \tilde{\mathbf{f}}.$$

For details, see [32, Ch. 25], as well as [4, 22, 26, 35].

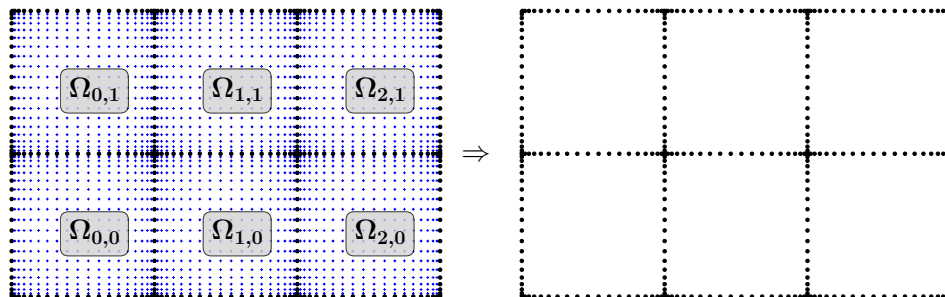


FIGURE 3. HPS is a multi-domain spectral collocation scheme where the PDE is enforced on each subdomain interior using dense spectral differentiation. Prior to interfacing with SlabLU, we "eliminate" the interior blue nodes in parallel and produce an equivalent system to solve on the boundaries. The original grid has $n_1 \times n_2$ points, and remaining grid has $\approx n_1 n_2 / p$ points.

Remark 1. A key point of the present work is that the solver has only two levels, which makes the “H” in “HPS” a slight misnomer, as it refers to “hierarchical”. We nevertheless stick with the “HPS” acronym to conform with the prior literature.

3. STAGE ONE: ELIMINATION OF NODES INTERIOR TO EACH SLAB

This section describes the process that we use to eliminate the nodes interior to each slab that we sketched out in Section 1.2. The objective is to reduce the sparse stiffness matrix \mathbf{A} (illustrated in Figure 1c) into the smaller block tridiagonal matrix \mathbf{T} (illustrated in Figure 1d). The techniques described form the core algorithmic innovation of the manuscript.

3.1. Schur complements. With the ordering introduced in Section 2.2, the coefficient matrix \mathbf{A} has the block form

$$(6) \quad \begin{bmatrix} \mathbf{A}_{11} & \mathbf{A}_{12} & \mathbf{0} & \mathbf{0} & \mathbf{0} & \dots \\ \mathbf{A}_{21} & \mathbf{A}_{22} & \mathbf{A}_{23} & \mathbf{0} & \mathbf{0} & \dots \\ \mathbf{0} & \mathbf{A}_{32} & \mathbf{A}_{33} & \mathbf{A}_{34} & \mathbf{0} & \dots \\ \mathbf{0} & \mathbf{0} & \mathbf{A}_{43} & \mathbf{A}_{44} & \mathbf{A}_{45} & \dots \\ \vdots & \vdots & \vdots & \vdots & \vdots & \vdots \end{bmatrix} \begin{bmatrix} \mathbf{u}_1 \\ \mathbf{u}_2 \\ \mathbf{u}_3 \\ \mathbf{u}_4 \\ \vdots \end{bmatrix} = \begin{bmatrix} \mathbf{f}_1 \\ \mathbf{f}_2 \\ \mathbf{f}_3 \\ \mathbf{f}_4 \\ \vdots \end{bmatrix}.$$

We eliminate the vectors $\mathbf{u}_2, \mathbf{u}_4, \mathbf{u}_6, \dots$ that represent unknown variables in the interior of each slab through a step of block Gaussian elimination. To be precise, we insert the relation

$$(7) \quad \mathbf{u}_i = \mathbf{A}_{ii}^{-1} (\mathbf{f}_i - \mathbf{A}_{i,i-1} \mathbf{u}_{i-1} - \mathbf{A}_{i,i+1} \mathbf{u}_{i+1}), \quad i = 2, 4, 6, \dots$$

into the odd-numbered rows in (6) to obtain the reduced system

$$(8) \quad \begin{bmatrix} \mathbf{T}_{11} & \mathbf{T}_{13} & \mathbf{0} & \mathbf{0} & \mathbf{0} & \dots \\ \mathbf{T}_{31} & \mathbf{T}_{33} & \mathbf{T}_{35} & \mathbf{0} & \mathbf{0} & \dots \\ \mathbf{0} & \mathbf{T}_{53} & \mathbf{T}_{55} & \mathbf{T}_{57} & \mathbf{0} & \dots \\ \mathbf{0} & \mathbf{0} & \mathbf{T}_{73} & \mathbf{T}_{75} & \mathbf{T}_{77} & \dots \\ \vdots & \vdots & \vdots & \vdots & \vdots & \vdots \end{bmatrix} \begin{bmatrix} \mathbf{u}_1 \\ \mathbf{u}_3 \\ \mathbf{u}_5 \\ \mathbf{u}_7 \\ \vdots \end{bmatrix} = \begin{bmatrix} \tilde{\mathbf{f}}_1 \\ \tilde{\mathbf{f}}_3 \\ \tilde{\mathbf{f}}_5 \\ \tilde{\mathbf{f}}_7 \\ \vdots \end{bmatrix},$$

where the sub-blocks of \mathbf{T} are defined as

$$(9) \quad \mathbf{T}_{11} = \mathbf{A}_{11} - \mathbf{A}_{12} \mathbf{A}_{22}^{-1} \mathbf{A}_{21},$$

$$(10) \quad \mathbf{T}_{13} = \mathbf{A}_{13} - \mathbf{A}_{12} \mathbf{A}_{22}^{-1} \mathbf{A}_{23},$$

$$(11) \quad \mathbf{T}_{31} = \mathbf{A}_{31} - \mathbf{A}_{32} \mathbf{A}_{22}^{-1} \mathbf{A}_{23},$$

$$(12) \quad \mathbf{T}_{33} = \mathbf{A}_{33} - \mathbf{A}_{32} \mathbf{A}_{22}^{-1} \mathbf{A}_{23} - \mathbf{A}_{34} \mathbf{A}_{44}^{-1} \mathbf{A}_{43},$$

$$(13) \quad \mathbf{T}_{35} = \mathbf{A}_{35} - \mathbf{A}_{34} \mathbf{A}_{44}^{-1} \mathbf{A}_{43},$$

and so on. The reduced right-hand sides $\tilde{\mathbf{f}}$ are defined as

$$(14) \quad \tilde{\mathbf{f}}_1 = \mathbf{f}_1 - \mathbf{A}_{12} \mathbf{A}_{22}^{-1} \mathbf{f}_2,$$

$$(15) \quad \tilde{\mathbf{f}}_3 = \mathbf{f}_3 - \mathbf{A}_{32} \mathbf{A}_{22}^{-1} \mathbf{f}_2 - \mathbf{A}_{34} \mathbf{A}_{44}^{-1} \mathbf{f}_4,$$

$$(16) \quad \tilde{\mathbf{f}}_5 = \mathbf{f}_5 - \mathbf{A}_{54} \mathbf{A}_{44}^{-1} \mathbf{f}_4 - \mathbf{A}_{56} \mathbf{A}_{66}^{-1} \mathbf{f}_6,$$

etc.

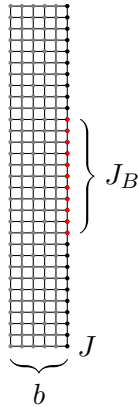


FIGURE 4. Contiguous set of points defined as $J_B \subset J$.

3.2. Rank structure in the reduced blocks. We next discuss algebraic properties of the blocks of the reduced coefficient matrix \mathbf{T}_{ij} that allow for \mathbf{T} to be formed efficiently. The sub-blocks of \mathbf{T} are Schur-complements of sparse matrices. For instance, block \mathbf{T}_{11} has the formula

$$(17) \quad \mathbf{T}_{11} = \begin{matrix} \mathbf{A}_{11} & - & \mathbf{A}_{12} & \mathbf{A}_{22}^{-1} & \mathbf{A}_{21} \\ n_2 \times n_2 & & n_2 \times n_2 & n_2 b \times n_2 b & n_2 b \times n_2 \end{matrix},$$

where $\mathbf{A}_{11}, \mathbf{A}_{12}, \mathbf{A}_{21}$ are sparse with $O(n_2)$ non-zero entries and \mathbf{A}_{22} is a sparse banded matrix. Factorizing \mathbf{A}_{22} can be done efficiently using a sparse direct solver, but forming $\mathbf{A}_{22}^{-1} \mathbf{A}_{21}$ naively may be slow and memory-intensive, especially considering that \mathbf{A}_{21} is sparse and would need to be converted to dense to interface with solve routines.

We use an alternate approach for efficiently forming \mathbf{T}_{11} that achieves high arithmetic intensity while maintaining a very low memory footprint. First, we prove algebraic properties about \mathbf{T}_{11} , which is a dense but structured matrix that only needs $O(n_2 b)$ storage in exact precision. The matrix \mathbf{T}_{11} is compressible in a format called Hierarchically Block-Separable (HBS) or Hierarchically Semi-Separable (HSS) with exact HBS rank at most $2b$. HBS matrices are a type of hierarchical matrix (\mathcal{H} -matrix), which allow dense matrices to be stored efficiently by exploiting low-rank structure in sub-blocks at different levels of granularity [5, 25, 32]. The matrices \mathbf{T}_{jk} are compressible in several \mathcal{H} -matrix formats, e.g. Hierarchical Off-Diagonal Low Rank (HODLR). The rank property of \mathbf{T}_{11} is formally stated in Proposition 3.2.

After establishing the HBS structure of \mathbf{T}_{11} , we then describe how this structure can be recovered with only $O(b)$ matrix vector products of \mathbf{T}_{11} and \mathbf{T}_{11}^* . Vectors can efficiently be applied because \mathbf{T}_{11} and its transpose are compositions of sparse matrices. Since \mathbf{T}_{11} is admissible as a HODLR matrix, the structure can be efficiently recovered from matrix-vector products in this format as well [29, 31], though more vectors are required for reconstruction in this format.

[Rank Property] Let J_B be a contiguous set of points on the slab interface J , and let J_F be the rest of the points $J_F = J \setminus J_B$. The sub-matrices $(\mathbf{T}_{11})_{BF}, (\mathbf{T}_{11})_{FB}$ have exact rank at most $2b$. See Figure 4 for an illustration of J_B . The proof is in Appendix A.

3.3. Recovering \mathcal{H} -matrix structure from matrix-vector products. We next describe how to extract an \mathcal{H} -matrix representation of the reduced blocks purely from matrix-vector products. For concreteness, we are trying to recover $\mathbf{T}_{11} \in \mathbb{R}^{n_2 \times n_2}$ as an HBS matrix with HBS rank at most $2b$. Typically, \mathcal{H} -matrices are used when the cost of forming or factorizing these matrices densely, is prohibitively large. In the context of SlabLU, $\mathbf{T}_{11} \in \mathbb{R}^{n_2 \times n_2}$ can be stored densely for the problem sizes of interest, but traditional methods for forming \mathbf{T}_{11}

densely may be inefficient, as described in Section 3.2. Instead, we recover \mathbf{T}_{11} as an HBS matrix with HBS rank at most $2b$ from matrix-matrix products

$$(18) \quad \underset{n_2 \times s}{\mathbf{Y}} = \underset{n_2 \times n_2}{\mathbf{T}_{11}} \underset{n_2 \times s}{\mathbf{\Omega}}, \quad \underset{n_2 \times s}{\mathbf{Z}} = \underset{n_2 \times n_2}{\mathbf{T}_{11}^*} \underset{n_2 \times s}{\mathbf{\Psi}},$$

where $\mathbf{\Omega}, \mathbf{\Psi}$ are Gaussian random matrices and $s = 6b$ using the algorithm presented in [27]. This is theoretically possible because an HBS matrix of size $n_2 \times n_2$ with HBS rank at most $2b$ can be encoded in $O(n_2b)$ storage. The HBS structure can be recovered from samples \mathbf{Y}, \mathbf{Z} after post-processing in $O(n_2b^2)$ flops. The algorithm presented in [27] can be seen as an extension of algorithms for recovering low-rank factors from random sketches [33]. A particular advantage of these algorithms is that they scale linearly and are truly black-box. The matrix-matrix products (18) are simple to evaluate using the matrix-free formula (17) of \mathbf{T}_{11} and its transpose. Applying \mathbf{T}_{11} involves two applications of sparse matrices and two triangular solves using pre-computed sparse triangular factors.

4. STAGE TWO: FACTORIZING THE REDUCED BLOCK TRIDIAGONAL COEFFICIENT MATRIX

The elimination of nodes interior to each slab that we described in Section 3 results in a reduced linear system

$$(19) \quad \mathbf{T}\tilde{\mathbf{u}} = \tilde{\mathbf{f}},$$

where $\tilde{\mathbf{u}}$ is the reduced solution vector and where $\tilde{\mathbf{f}}$ is the equivalent body load on slab interfaces I_1, I_3, \dots . We recall that the matrix \mathbf{T} is of size roughly $N/b \times N/b$, and is block tridiagonal with blocks of size $n_2 \times n_2$. Solving a system involving a block tridiagonal matrix is straight-forward using a blocked version of Gaussian elimination. In Algorithms 1 and 2 we summarize a basic scheme for solving (19) where we separate the process of Gaussian elimination into a ‘‘build stage’’ where we explicitly form and invert the Schur complements that arise in the Gaussian elimination, and a ‘‘solve stage’’ where the computed inverses are used to solve (19) for a given right hand side.

Algorithm 1: Sweeping build stage.

Given a block-tridiagonal matrix \mathbf{T} , Algorithm 1 builds a direct solver for \mathbf{T} , with the result stored in the matrices $\mathbf{S}_1, \mathbf{S}_3, \dots$

```

1  $\mathbf{S}_1 \leftarrow \mathbf{T}_{11}$ ;
2 for  $j = 2, \dots, n_1/b$  do
3    $\mathbf{S}_{2j+1} \leftarrow \mathbf{T}_{2j+1,2j+1} - \mathbf{T}_{2j+1,2j-1}\mathbf{S}_{2j-1}^{-1}\mathbf{T}_{2j-1,2j+1}$ ;
4   Store  $\mathbf{S}_{2j-1}^{-1}$ ;

```

Algorithm 2: Sweeping solve.

Given a body load $\tilde{\mathbf{f}}$ and precomputed inverses of $\mathbf{S}_1, \mathbf{S}_3, \dots$, Algorithm 2 computes the solution vector $\tilde{\mathbf{u}}$.

```

1  $\mathbf{y}_1 \leftarrow \mathbf{S}_1^{-1}\tilde{\mathbf{f}}_1$ ;
2 for  $j = 1, \dots, n_1/b$  do
3    $\mathbf{y}_{2j+1} \leftarrow \mathbf{S}_{2j+1}^{-1} \left( \tilde{\mathbf{f}}_{2j+1} - \mathbf{T}_{2j+1,2j-1}\mathbf{y}_{2j-1} \right)$ ;
4    $\tilde{\mathbf{u}}_{2n_1/b+1} \leftarrow \mathbf{S}_{2n_1/b+1}^{-1}\mathbf{y}_{2n_1/b+1}$ ;
5 for  $j = n_1/b, n_1/b - 1, \dots, 1$  do
6    $\tilde{\mathbf{u}}_{2j-1} \leftarrow \mathbf{S}_{2j-1}^{-1} \left( \mathbf{y}_{2j-1} - \mathbf{T}_{2j-1,2j+1}\tilde{\mathbf{u}}_{2j+1} \right)$ ;

```


We observe that the elimination process described in Section 3 automatically results in blocks that are represented in the HBS format. The most elegant way to solve (19) is to maintain the HBS format throughout Algorithms 1 and 2, as this leads to a solver with linear complexity in the case where the PDE is kept fixed as N increases. However, we have found that for two dimensional problems, dense linear algebra is fast enough that the most efficient way to solve (19) in practice is to simply convert the HBS matrix representation to dense matrices, and carry out all computations by brute force. (In the 3D version of SlabLU, rank structure must be exploited, however.)

Remark 2. *In the case where (1) has oscillatory solutions, and the number of points per wavelength is kept fixed as N increases, it is still possible to exploit rank structure in the blocks of \mathbf{T} . However, the ranks will grow during the execution of Algorithm 1. To minimize rank-growth, an odd-even elimination order can be used instead of the sequential one in Algorithm 1, but the method would still not attain linear complexity. We observe that our conversion to dense linear algebra allows us to side-step this complication, as our method relies on the sparsity pattern of the original matrix only.*

5. ALGORITHM AND COMPLEXITY COSTS

In this section, we provide a summary of the proposed algorithm, and discuss its efficient parallelization using batched linear algebra on a GPU. We also analyze the complexity costs, and choose the buffer size b as a function of the number of grid points $N = n_1 n_2$, in order to balance costs and achieve competitive complexities for the build and solve times. While our discussion on choosing b focuses on the 5-point stencil model problem, the conclusions are generally applicable to other discretizations.

We briefly summarize the algorithm for SlabLU. In Stage One, we compute factorizations of the form

$$(20) \quad \mathbf{A}_{22}^{-1}, \mathbf{A}_{44}^{-1}, \dots$$

$n_2 b \times n_2 b$ $n_2 b \times n_2 b$

for n_1/b sparse matrices. The reduced matrix \mathbf{T} is constructed using efficient black-box algorithms that recover \mathbf{T}_{jk} in HBS format through a random sampling method, as discussed in Section 3.3. It is important to note that Stage One can be trivially parallelized for each slab. In Stage Two, dense linear algebra is used to factorize \mathbf{T} as discussed in Section 4.

Algorithm 3 outlines how to use the computed factorization of \mathbf{A} to solve systems (3). This requires storing the sparse factorizations (20) and the factorization of \mathbf{T} .

Algorithm 3: Solving $\mathbf{A}\mathbf{u} = \mathbf{f}$ using computed direct solver.

- 1 Calculate the equivalent body $\tilde{\mathbf{f}}$ on I_1, I_3, \dots using (14-16) in parallel.
// Parallel computation
- 2 Solve $\mathbf{T}\tilde{\mathbf{u}} = \tilde{\mathbf{f}}$ for $\tilde{\mathbf{u}}$ on I_1, I_3, \dots using Algorithm 2.
// Serial algorithm
- 3 Solve for \mathbf{u} on I_2, I_4, \dots using $\tilde{\mathbf{u}}$ on I_1, I_3, \dots with (7) in parallel.
// Parallel computation

5.1. Ease of Parallelism and Acceleration with Batched Linear Algebra. We highlight the features of the SlabLU scheme that make it particularly suitable for implementation on GPUs and compare it to multi-level nested dissection schemes. Although nested dissection is work-optimal for minimizing the fill-in of the computed factorization, parallelizing it for high performance on GPUs remains an active area of research. Recent results include the GPU-accelerated multifrontal algorithm proposed in [21], which splits the problem into

independent sub-problems that can be factorized entirely in GPU memory. The factorization is then performed using a level-by-level traversal with custom hand-coded kernels for small matrices and vendor-optimized BLAS libraries for larger matrices.

However, there are significant challenges and avenues for improvement. Efficient nested dissection codes require parallel operations on a wide range of matrix sizes, and fully exploiting the potential of modern GPUs would require careful load balancing and memory access patterns [39]. Sparse direct solvers generally do not make use of batched linear algebra, a highly optimized framework for parallelized BLAS operations on many small matrices, because the framework is limited to matrices of the same size, and variable-sized batching is often needed in the context of a sparse direct solver. Although an extension to variable sizes is currently under development [1], it is far less mature than its constant-sized counterpart.

In contrast, the SlabLU scheme takes advantage of the two-level structure to simplify the optimization process significantly. The trade-off is a small asymptotic increase in the flop and memory complexity of the algorithm, but there are large benefits in terms of practical performance on GPUs. SlabLU only requires factorizing two front sizes: b in Stage One and n_2 in Stage Two. Since the scheme has only two levels, it is relatively easy to optimize the data movement and coordination between the GPU, which has limited memory, and the CPU.

In Stage One, parallel operations are performed on many small matrices, while in Stage Two, serial operations are performed on a relatively small number of larger matrices. Our implementation makes use of highly optimized libraries (e.g., MAGMA for batched linear algebra on small matrices and vendor-optimized BLAS for large matrices), and the high practical performance required little, if any, hand tuning. Stage One also provides an opportunity to incorporate highly optimized batched linear algebra schemes by using matrix-free randomized algorithms to recover \mathbf{T}_{jk} in HBS format, as we do in our implementation. \mathcal{H} -matrix algebras can be efficiently parallelized using batched linear algebra because the off-diagonal rank is small and uniform on each level of the \mathcal{H} -matrix structure [8, 11].

Overall, the SlabLU scheme offers a more straightforward path to optimizing sparse direct solvers on modern GPUs than traditional nested dissection codes. While parallelizing nested dissection codes remains an active area of research, the simplicity of SlabLU makes it an attractive option for efficient parallelization of sparse direct solvers.

5.2. Choosing the buffer size b . The buffer size is chosen to balance the costs of Stage One and Stage Two. Stage One involves computing sparse factorizations (20), where each sparse matrix is banded with bandwidth b . This process requires $\frac{n_1}{b} \times O(b^3 n_2)$ flops. The cost of constructing \mathbf{T}_{jk} in HBS format is dominated by the cost of constructing the random samples (18), which requires $O(n_2 b^3)$ flops using matrix-free formulas for applying \mathbf{T}_{jk} . The cost of post-processing random samples is asymptotically small. To summarize, Stage One is dominated by the costs of the factorizations of sparse matrices (20) and constructing random samples (18), which both have costs $\frac{n_1}{b} \times O(n_2 b^4) = O(b^3 N)$. Importantly, Stage One can be done in parallel for n_1/b sub-domains.

Stage Two involves a simple sweeping factorization of \mathbf{T} using Algorithm 1. The reduced matrix \mathbf{T} has $\approx n_1/b$ blocks, each of size $n_2 \times n_2$. The total cost of constructing the factorization is

$$(21) \quad T_{\text{build}} = \underset{\text{Stage One}}{O(b^2 N)} + \underset{\text{Stage Two}}{O\left(\frac{1}{b} n_1 n_2^3\right)}.$$

To balance the costs of Stage One and Stage Two, we choose $b = O\left(n_2^{2/3}\right)$. The total cost of the build stage is $T_{\text{build}} = O\left(n_1 n_2^{7/3}\right)$.

To apply the direct solver for \mathbf{A} , one needs to store the sparse factorizations (20) and the direct solver for \mathbf{T} . The sparse factorizations (20) require $O\left(\frac{n_1}{b} \times b^2 n_2\right)$ storage, and storing the direct solver for \mathbf{T} requires $O\left(\frac{n_1}{b} \times n_2^2\right)$ storage. With the choice of $b = O\left(n_2^{2/3}\right)$, the sparse factorizations require asymptotically more space to store. We can rebalance the memory costs of Stage One and Stage Two by using a nested dissection ordering for the sparse factorization within each slab or by “discarding” some of the factorization in Stage One (e.g. corresponding to small subdomains) and re-factorizing as needed to apply Algorithm 3. Then the memory costs are

$$(22) \quad T_{\text{solve}} = \frac{n_1}{b} \times O\left(n_2^2\right) = O\left(n_1 n_2^{4/3}\right).$$

Our implementation also exploits rank-structures (e.g. in the off-diagonal sub-blocks of \mathbf{T}) to efficiently store the computed direct solver.

The algorithm scales particularly well for domains with high aspect ratio when $n_1 > n_2$. A square domain is the adversarial worst case in terms of the algorithm complexity. When $n_1 = n_2$, then

$$(23) \quad T_{\text{build}} = O\left(N^{5/3}\right), \quad T_{\text{solve}} = O\left(N^{7/6}\right).$$

5.3. Complexity Analysis for SlabLU with HPS discretization. The numerical results feature a high order discretization scheme that interfaces particularly well with sparse direct solvers which we use to resolve high frequency scattering problems to high accuracy. As discussed in Section 2.3, HPS is a spectral collocation discretization that employs multiple subdomains to enforce the PDE using spectral differentiation. The subdomains are coupled together by ensuring continuity of the solution and its derivative across subdomains. A natural approach to factorizing the sparse coefficient matrix is to first factorize each leaf subdomain in parallel and then solve the remaining sparse matrix $\tilde{\mathbf{A}}$. The total cost of factorizing a sparse matrix arising from the HPS discretization can be expressed as

$$(24) \quad T_{\text{build}} = O\left(\underset{\text{leaf operations}}{p^4 N} + \underset{\text{direct solver}}{N^{5/3}} \right),$$

where N is the total number of unknowns and p is the polynomial degree used in the spectral collocation method. Traditionally, the pre-factor cost of the leaf operations has been considered prohibitively expensive. However, [43] describes simple GPU optimizations that use batched linear algebra to significantly accelerate the leaf operations. The results are particularly compelling for p up to 42. Numerical experiments presented in [43] demonstrate that the choice of p does not have a significant impact on the time required to factorize the sparse matrix. This means that p can be chosen based on physical considerations rather than practical concerns.

Remark 3. *The leaf operations are so efficient that we can save on storage costs by not explicitly storing the factorizations of the local spectral differentiation matrices in each HPS subdomain. Instead, we can reform and refactor these matrices as needed, and these costs are included in the solve time reported in Section 6.3.*

6. NUMERICAL EXPERIMENTS

In this section, we demonstrate the effectiveness of our solver through a series of numerical experiments. We report the build time, solve time, and accuracy of solving constant and variable-coefficient elliptic PDEs using two collocation-based discretization schemes on both rectangular and curved geometries. Our experiments were conducted on various hardware architectures to showcase the portability and ease of performance tuning of our framework.

Our experiments compare SlabLU to SuperLU in the factorization of a PDE discretized with 2nd order finite differences. The results demonstrate that SlabLU achieves a significant speedup compared to traditional nested dissection schemes, even without GPU acceleration.

Additionally, we utilize a high-order multidomain spectral collocation scheme, briefly introduced in Section 2.3, to solve challenging scattering phenomena. The high-order discretization scheme allows us to accurately discretize the PDE, while the flexibility of the multidomain scheme enables us to solve PDEs on curved domains using SlabLU. The combination of SlabLU and high-order discretization provides a powerful tool for simulating electromagnetic and acoustic scattering. Our focus is on physical phenomena that may be beyond the reach of preconditioned iterative methods.

6.1. Description of Benchmark PDEs and Accuracies Reported. We briefly describe the PDEs with manufactured solutions used as benchmarks in our numerical experiments and how we calculate accuracy. The first PDE is the Laplace equation

$$(25) \quad \begin{cases} -\Delta u(x) = 0, & x \in \Omega, \\ u(x) = u_{\text{true}}(x), & x \in \Gamma, \end{cases}$$

The Dirichlet data is the restriction of the true analytic solution to the boundary

$$(26) \quad u_{\text{true}}(x) = \log(\|x - (-0.1, 0.5)\|).$$

The second PDE is a constant coefficient Helmholtz problem

$$(27) \quad \begin{cases} -\Delta u(x) - \kappa^2 u(x) = 0, & x \in \Omega, \\ u(x) = u_{\text{true}}(x), & x \in \Gamma, \end{cases}$$

where the true solution u_{true} is given by

$$(28) \quad u_{\text{true}} = J_0(\kappa\|x - (-0.1, 0.5)\|),$$

where $x \mapsto J_0(\kappa|x|)$ is the zeroth Bessel function of the first kind.

After applying the direct solver, we obtain the calculated solution \mathbf{u}_{calc} at discretization points within the domain. We report the relative error with respect to the residual of the discretized system (3) and with respect to the true solution \mathbf{u}_{true} evaluated at the collocation points as follows:

$$(29) \quad \text{relerr}_{\text{res}} = \frac{\|\mathbf{A}\mathbf{u}_{\text{calc}} - \mathbf{f}\|_2}{\|\mathbf{f}\|_2}, \quad \text{relerr}_{\text{true}} = \frac{\|\mathbf{u}_{\text{calc}} - \mathbf{u}_{\text{true}}\|_2}{\|\mathbf{u}_{\text{true}}\|_2}.$$

We also report T_{factor} , which is the wall-clock time needed to factorize the coefficient matrix \mathbf{A} , and M_{factor} , which is the memory required to store the computed direct solver. Additionally, we report T_{solve} , which is the time needed to apply the direct solver to solve systems (3), as described in Algorithm 3. Unless otherwise stated, the solve is done entirely on the CPU for a single right hand side vector.

6.2. Experiments using Low-Order Discretization. In this section, we demonstrate how SlabLU performs on sparse coefficient matrices arising from PDEs discretized with 2nd order finite differences. We also compare SlabLU to SuperLU, an existing multi-level nested dissection code.

We conducted the experiments on three different architectures: (1) a 16-core Intel i9-12900k CPU with 128 GB of RAM, (2) an NVIDIA RTX 3090 GPU with 24 GB of memory and access to 128 GB of RAM, and (3) an NVIDIA V100 with 32 GB of memory and access to 768 GB of RAM. We chose to run experiments on architectures (1) and (2) to demonstrate that the memory volume required to run SlabLU is reasonable.

All experiments used double precision. While the RTX 3090 supports double precision calculations, its peak performance using fp64 is significantly less than that of fp32. In comparison, the V100 is designed for high performance with fp64. Surprisingly, we found that the timings on the two systems did not differ significantly. We observed significant speedups for Stage Two on the V100 compared to the RTX 3090, but little change for Stage One, leading us to conclude that the factorization of \mathbf{T} is compute-bound, whereas the sparse factorizations in Stage One are latency-bound.

We demonstrate competitive scaling for the build time of the factorization and for the memory footprint. See Figure 5 for the Poisson equation (25) and Figure 6 for the constant-coefficient Helmholtz equation (27). Despite the super-linear complexity scaling, the scaling appears to be linear for grids of size up to $N = 100\text{M}$. However, for coercive PDEs, there is rarely a reason to scale the discretizations to such large grids. For the Helmholtz equation, we discretize to at least 10 points per wavelength to resolve the oscillatory solutions, leading to large grids. However, due to the effect of pollution when using low-order discretization, we need to discretize the Helmholtz equation to 250 points per wavelength to attain 3 digits of accuracy with respect to the known analytic solution.

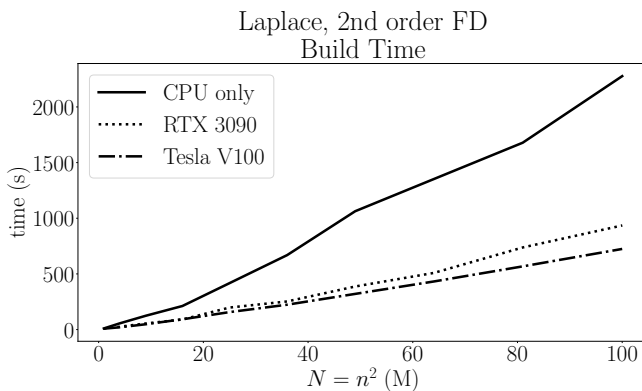


FIGURE 5. Timing results for solving Poisson equation with a body load (eq. 25) using a 2nd order finite difference discretization. Though the build time of SlabLU scales as $O(N^{5/3})$, the observed asymptotic behavior has linear scaling with N . The table reports how b grows as a function of the problem size N .

N	b	M_{factor}	T_{solve}	$\text{relerr}_{\text{res}}$	$\text{relerr}_{\text{true}}$
1.0 M	50	0.5 GB	0.5 s	1.99e-12	5.22e-07
4.0 M	100	2.5 GB	1.6 s	3.41e-12	1.31e-07
9.0 M	125	6.5 GB	3.6 s	4.78e-12	5.81e-08
16.0 M	160	12.9 GB	7.3 s	4.15e-12	3.27e-08
25.0 M	200	22.5 GB	12.2 s	4.66e-12	2.09e-08
36.0 M	200	32.7 GB	18.2 s	5.90e-12	1.46e-08
49.0 M	200	46.8 GB	27.4 s	1.10e-11	1.04e-08
64.0 M	250	63.9 GB	37.7 s	6.08e-12	8.10e-09
81.0 M	250	83.3 GB	55.3 s	6.16e-12	6.32e-09
100.0 M	250	105.6 GB	65.4 s	7.96e-12	4.92e-09

Sparse direct solvers use sparsity in the discretized operator in order to factorize the sparse coefficient matrix exactly. SlabLU uses sparsity in the traditional sense for the sparse factorizations (20) in Stage One. In order to construct the reduced coefficient matrix \mathbf{T} , we prove a rank property in Proposition (3.2) that allows us to represent sub-blocks $\mathbf{T}_{jk} \in \mathbb{R}^{n_2 \times n_2}$ *exactly* in $O(n_2 b)$ storage and recover \mathbf{T}_{jk} in HBS format using random sampling; see Section 3.3. Crucially, Proposition (3.2) is a purely algebraic property that holds regardless of the PDE. Often, the HBS rank of \mathbf{T}_{jk} is considerably less than $2b$; SlabLU uses adaptive rank sampling in the HBS construction to considerably save on build time and storage costs. For a thin slab with λ wavelengths in the thin dimension, we have observed that the ranks are roughly twice λ plus a small constant factor. For the Poisson equation, HBS rank about 50 approximates \mathbf{T}_{jk} to high accuracy.

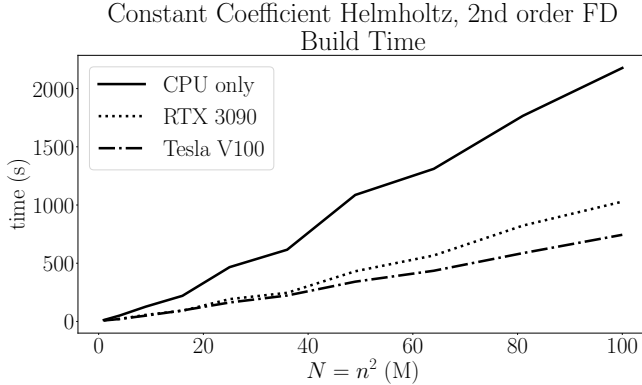


FIGURE 6. Timing results for solving the constant coefficient Helmholtz equation (27) using a 2nd order finite difference discretization. The wavenumber κ is increased with the problem size to maintain 250 points per wavelength. Though the solution is resolved to at least 10 digits in the residual, the relative error compared to the true solution is only 3 digits.

We compare the performance of SlabLU and SuperLU in solving the 2nd order finite difference discretization of the constant coefficient Helmholtz equation (27), which results in very ill-conditioned sparse matrices (3) that need to be solved.

SuperLU is a generic sparse direct solver that computes a sparse LU factorization of any given sparse matrix to high accuracy. It uses groupings of nodes into "supernodes" to leverage BLAS3 operations on dense sub-blocks [7, 28] and is computed with the default permutation specification of COLAMD ordering to minimize fill-in.

We use the Scipy interface (version 1.8.1) to call SuperLU. During the factorization, SuperLU may pivot between sub-blocks to achieve stability in the computed factorization, resulting in superior accuracy in the residual. Despite limitations in the pivoting scheme of SlabLU, both schemes are able to resolve the solution up to the discretization error (see Figure 7). However, our comparison shows that SlabLU outperforms SuperLU in terms of build times and memory costs up to about 10M points. It is somewhat surprising that SlabLU outperforms SuperLU in terms of memory costs; we believe this is because SuperLU stores its computed factorization in sparse CSR format, leading to large storage costs for dense sub-blocks. For problems larger than 10.2M points, SuperLU does not compute the factorization, likely because the memory requirements exceed some pre-prescribed limit.

6.3. Solving Challenging Scattering Problems with High Order Discretization.

High-order discretization is crucial for resolving variable-coefficient scattering phenomena due to the pollution effect, which requires increasing the number of points per wavelength as the domain size increases [6, 14]. The HPS discretization (cf. Section 2.3) is less sensitive to pollution because it allows for a high choice of local polynomial order [23, 30]. In Helmholtz experiments, HPS with $p = 22$ accurately resolves oscillatory solutions using only 10 points per wavelength on domains up to size $1000\lambda \times 1000\lambda$, while 2nd order FD requires 100-250 points per wavelength to achieve low accuracy. Combining HPS with SlabLU provides a powerful tool for resolving challenging scattering phenomena to high accuracy, especially for situations where efficient preconditioners are not available [17]. We first demonstrate the performance of SlabLU for sparse coefficient matrices arising from the HPS discretization on

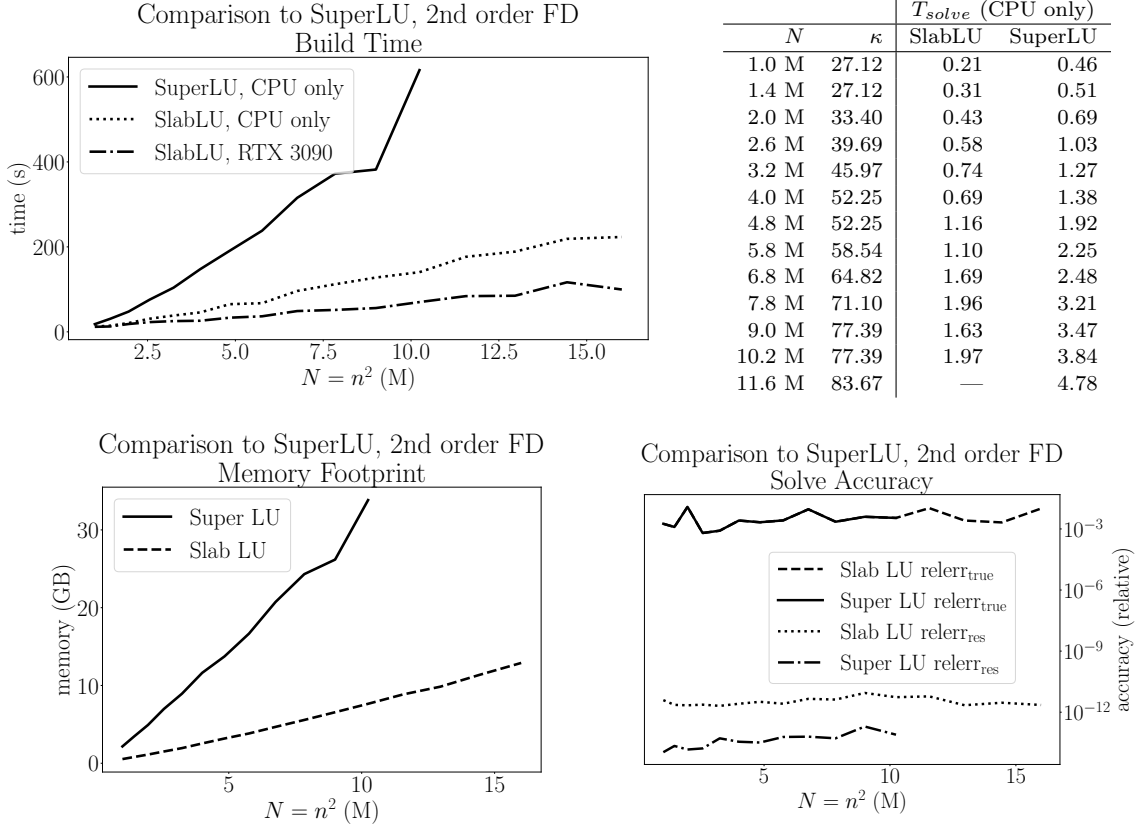


FIGURE 7. Comparison to Super LU for 2d order FD. SlabLU groups nodes into supernodes to leverage batched BLAS3 operations in Stage One and uses GPU acceleration for the large fronts in Stage Two. For the CPU-comparison, SlabLU is faster by a factor of 4 for $N=10.2M$. Using GPU acceleration makes the method faster by a factor of 8. Additionally, SlabLU is more memory efficient by a factor of 4 for $N = 10.2 M$.

a benchmark PDE of constant coefficient Helmholtz in Figure 8. As discussed in Section 5.3, the leaf operations are handled efficiently using batched linear algebra, and the local leaf factorizations are discarded and re-factorized as needed during the solve stage to save on memory costs for the direct solver.

We will now demonstrate the ability of HPS, combined with SlabLU as a sparse direct solver, to solve complex scattering phenomena on various 2D domains. For the presented PDEs, we will show how the accuracy of the calculated solution converges to a reference solution depending on the choice of p in the discretization. Specifically, we will solve the BVP (1) with the variable-coefficient Helmholtz operator (2) for Dirichlet data on curved and rectangular domains.

We fix the PDE and refine the mesh to compare calculated solutions to a reference solution obtained on a fine mesh with high p , as the exact solution is unknown. The relative error is calculated by comparing \mathbf{u}_{calc} to the reference solution \mathbf{u}_{ref} at a small number of collocation points $\{x_j\}_{j=1}^M$ using the l_2 norm

$$(30) \quad \text{relerr}_{\text{approx}} = \frac{\|\mathbf{u}_{\text{calc}} - \mathbf{u}_{\text{ref}}\|_2}{\|\mathbf{u}_{\text{ref}}\|_2}.$$

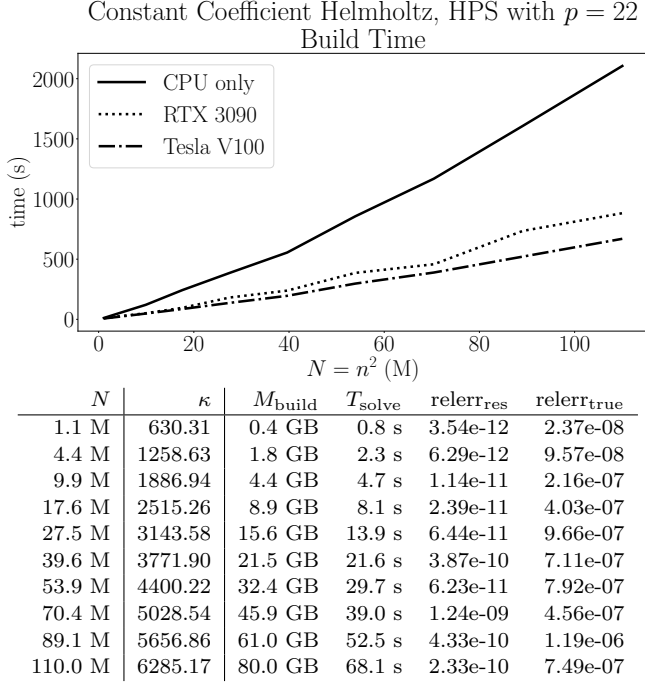


FIGURE 8. Timing results for solving the constant coefficient Helmholtz equation (eq. 27) using an HPS discretization with $p = 22$. The wavenumber κ is increased with the problem size to maintain 10 points per wavelength. Using a high order multidomain spectral collocation scheme allows us to avoid the effects of pollution and achieve at least 6 digits of relative accuracy, compared to the known solution.

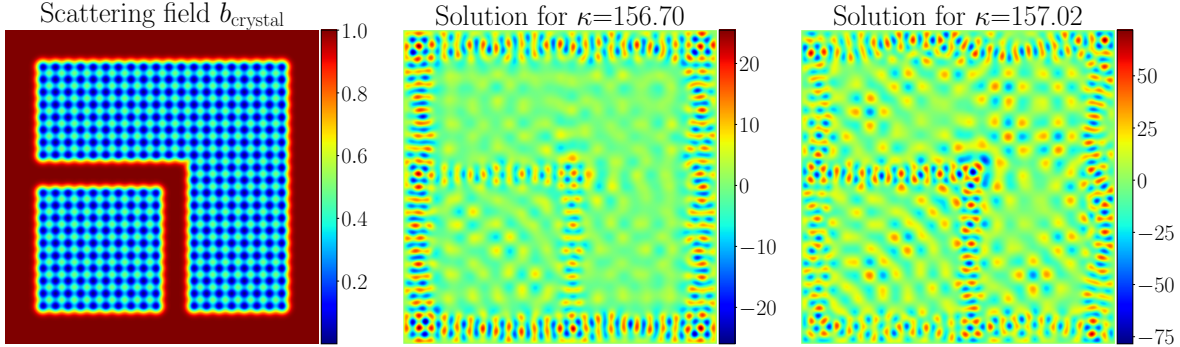


FIGURE 9. Solutions of variable-coefficient Helmholtz problem on square domain Ω with Dirichlet data given by $u \equiv 1$ on $\partial\Omega$ for various wavenumbers κ . The scattering field is b_{crystal} , which is a photonic crystal with an extruded corner waveguide. The crystal is represented as a series of narrow Gaussian bumps with separation $s = 0.04$ and is designed to filter wave frequencies that are roughly $1/s$.

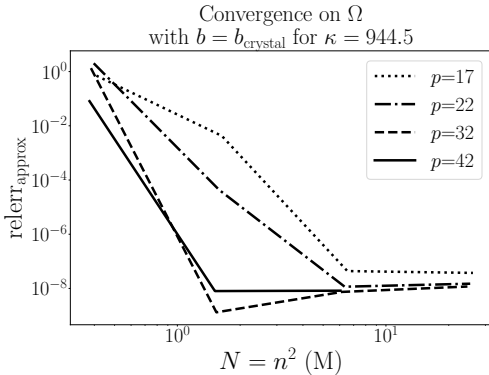


FIGURE 10. Convergence on square domain Ω for reference solution \mathbf{u}_{ref} on HPS discretization for $N=36\text{M}$ with $p = 42$.

We demonstrate the convergence on a unit square domain $\Omega = [0, 1]^2$ with a variable coefficient field b_{crystal} corresponding to a photonic crystal, shown in Figure 9. The convergence plot is presented in Figure 10.

Next, we show the convergence on a curved domain Ψ with a constant-coefficient field $b \equiv 1$, where Ψ is a half-annulus given by an analytic parameterization over a reference rectangle. The domain Ψ is parametrized as

$$(31) \quad \Psi = \left\{ \left(\cos \left(\hat{\theta}(x_1) \right), \sin \left(\hat{\theta}(x_1) \right) \right) \text{ for } (x_1, x_2) \in [0, 3] \times [0, 1] \right\},$$

where $\hat{\theta}(z) = \frac{\pi}{3}z$. Using the chain rule, (2) on Ψ takes a different form of a variable-coefficient elliptic PDE on the reference rectangle. The solutions on Ψ are shown in Figure 11, and the convergence plot is presented in Figure 12.

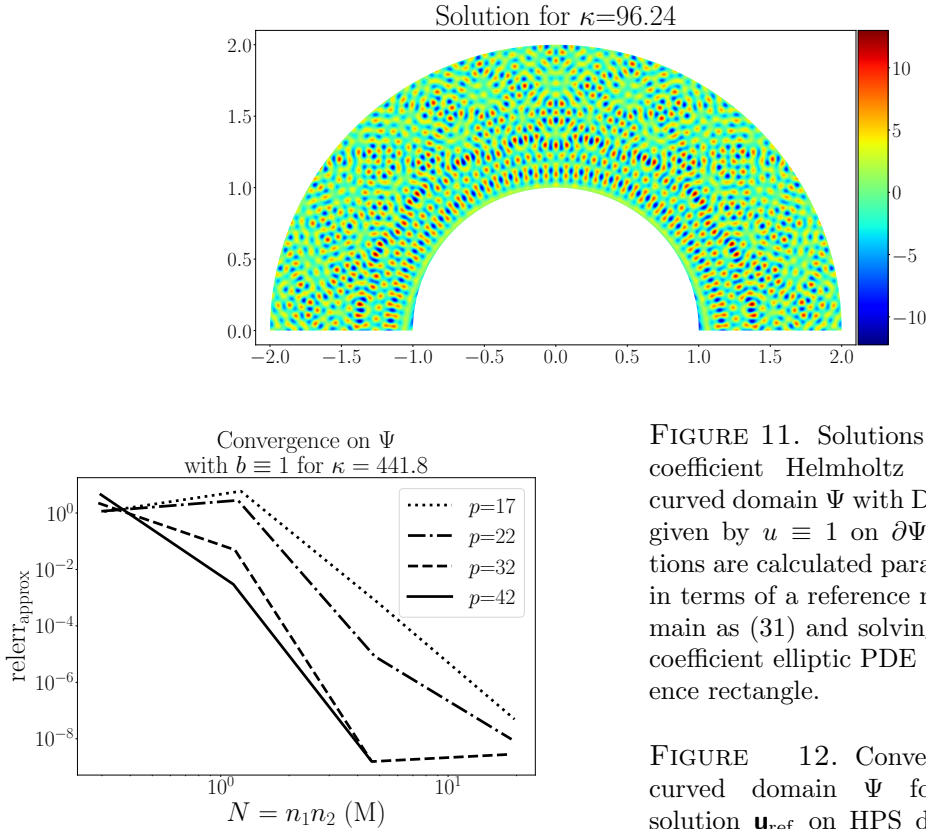


FIGURE 11. Solutions of constant-coefficient Helmholtz problem on curved domain Ψ with Dirichlet data given by $u \equiv 1$ on $\partial\Psi$. The solutions are calculated parametrizing Ψ in terms of a reference rectangle domain as (31) and solving a variable-coefficient elliptic PDE on the reference rectangle.

FIGURE 12. Convergence on curved domain Ψ for reference solution \mathbf{u}_{ref} on HPS discretization for $N=36\text{M}$ with $p = 42$.

Finally, we demonstrate convergence on a curved domain Φ with a constant coefficient field $b \equiv 1$, where we have implemented a periodic boundary condition. The domain Φ is parametrized by the formula

$$(32) \quad \Phi = \left\{ \left(\hat{r}(x_1, x_2) \cos \left(\hat{\theta}(x_1) \right), \hat{r}(x_1, x_2) \sin \left(\hat{\theta}(x_1) \right) \right) \text{ for } (x_1, x_2) \in [0, 6] \times [0, 1] \right\},$$

where $\hat{r}(z_1, z_2) = 1 + \frac{1}{5} \cos \left(\frac{15}{\pi} z_1 + z_2 \right)$ and $\hat{\theta}(z) = \frac{\pi}{3}z$. By applying the chain rule, the Helmholtz operator (2) on Φ takes a different form of a variable-coefficient elliptic PDE on the reference rectangle. The solutions on Φ are illustrated in Figure 13, and the convergence plot is presented in Figure 14.

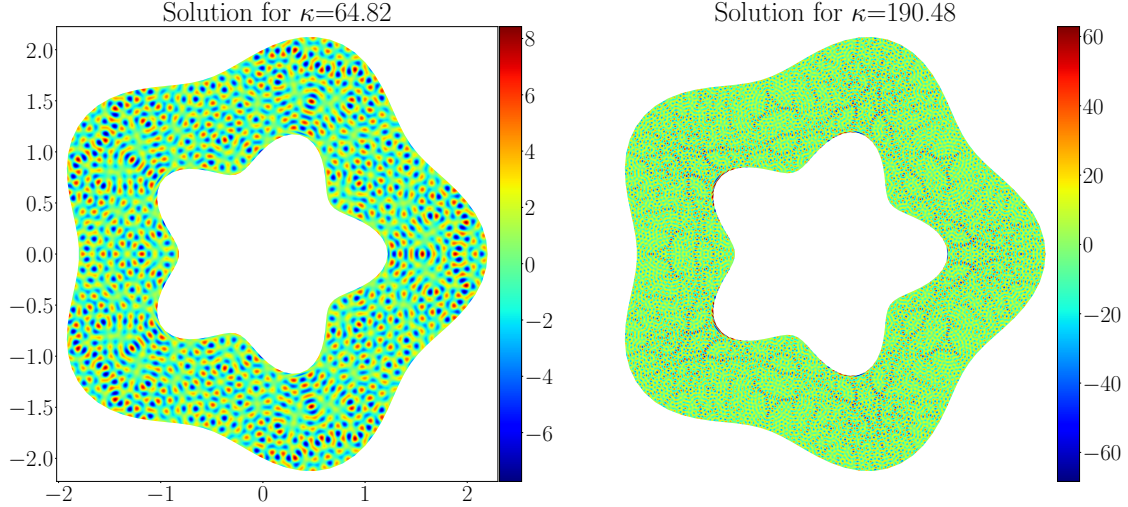


FIGURE 13. Solutions of constant-coefficient Helmholtz problem on curved domain Φ with Dirichlet data given by $u \equiv 1$ on $\partial\Phi$ for various wavenumbers κ .

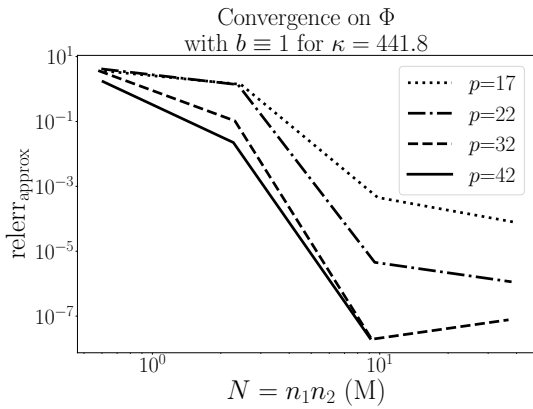


FIGURE 14. Convergence on curved domain Φ for reference solution \mathbf{u}_{ref} on HPS discretization for $N=36\text{M}$ with $p = 42$. Choosing high orders of p aids in the convergence.

7. CONCLUSION

This paper introduces SlabLU, a sparse direct solver framework designed for solving elliptic PDEs. The approach decomposes the domain into a sequence of thin slabs. The degrees of freedom internal to each slab are eliminated in parallel, yielding a reduced matrix \mathbf{T} defined on the slab interfaces. The reduced matrix \mathbf{T} is then factorized directly. The general two-level framework of SlabLU is simple to implement, easy to parallelize, and can be accelerated via batched linear algebra and GPU computations.

One key innovation of the method is the use of randomized compression with a sparse direct solver to efficiently form \mathbf{T} . The dense sub-blocks of \mathbf{T} have exact rank deficiencies in the off-diagonal blocks present in both the non-oscillatory and oscillatory regimes. The use of randomized black-box algorithms provides a purely algebraic means of efficiently forming \mathbf{T} for a variety of PDE discretizations. SlabLU requires $O(N^{5/3})$ time to build and $O(N^{7/6})$ time to apply.

The numerical experiments presented in this paper demonstrate that SlabLU is highly effective when used in conjunction with high-order multi-domain spectral collocation schemes. The combination of SlabLU with high order discretization enables the rapid and accurate simulation of large-scale and challenging scattering phenomena on both rectangular and curved domains to high accuracy.

The technique presented can readily be adapted to other standard discretization schemes such as finite element and finite volume methods. Less regular meshes can in principle be handled, although this would make some of the accelerations that we deploy less effective.

We are currently working to further accelerate SlabLU in two regards:

- (1) By maintaining a rank structured format for the blocks in the reduced coefficient matrix \mathbf{T} , the memory footprint of the scheme is reduced. Moreover, such a shift gives the scheme linear complexity in the regime where the PDE is kept fixed as N increases. (As opposed to the “fixed number of points per wavelength” scaling that is the gold standard for oscillatory problems.)
- (2) By replacing the sequential solve in the factorization of the reduced coefficient matrix \mathbf{T} by an odd-even ordering where every other block is eliminated in a hierarchical fashion, much higher parallelism can be attained.

Both accelerations would in principle be helpful for 2D problems, but a key point of the current manuscript is that neither turned out to be necessary – very high efficiency and essentially linear scaling is maintained up to $N \approx 10^8$. In *three dimensions*, however, the situation is different. Here the blocks in the reduced coefficient matrix \mathbf{T} hold $\approx N^{2/3}$ nodes, versus $\approx N^{1/2}$ in 2D. This forces us to maintain the rank structured representations of these blocks throughout the computation, in part for purposes of computational speed, but primarily to keep storage requirements from becoming excessive. The extension of SlabLU to 3D is in progress, but tentative numerical experiments demonstrate excellent scalability in both shared and distributed memory environments. This work will be reported at a later time.

Acknowledgements Anna would like to thank her dad, Andriy, for gifting her the RTX-3090 GPU.

Funding The work reported was supported by the Office of Naval Research (N00014-18-1-2354), by the National Science Foundation (DMS-1952735 and DMS-2012606), and by the Department of Energy ASCR (DE-SC0022251).

APPENDIX A. RANK PROPERTY OF THIN SLABS

In this appendix, we prove Proposition 3.2, which makes a claim on the rank structure of \mathbf{T}_{11} , defined in (17). [Rank Property] Let J_B be a contiguous set of points on the slab interface J , and let J_F be the rest of the points $J_F = J \setminus J_B$. The sub-matrices $(\mathbf{T}_{11})_{BF}$, $(\mathbf{T}_{11})_{FB}$ have exact rank at most $2b$.

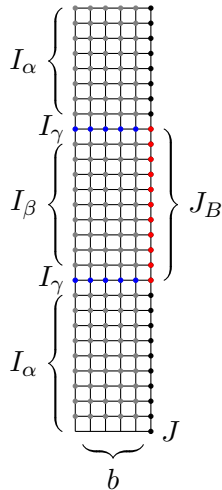


FIGURE 15. To assist in the proof of Proposition 3.2, we define a partitioning of the slab interface $J = J_B \cup J_F$, where $J_F = J \setminus J_B$. We also partition the slab interior nodes into $I_\alpha \cup I_\beta \cup I_\gamma$.

Recall that $\mathbf{T}_{11} = \mathbf{A}_{11} - \mathbf{A}_{12}\mathbf{A}_{22}^{-1}\mathbf{A}_{21}$. The proof relies on the sparsity structure of the matrices in the Schur complement. As stated in the proposition, the slab interface I_1 is partitioned into indices I_B and I_F . The proof relies on partitioning I_2 as well, into the indices $I_\alpha, I_\beta, I_\gamma$ shown in Figure 15, where $|I_\gamma| = 2b$.

The matrix $\mathbf{A}_{2,2}$ is sparse and can be factorized as

$$(33) \quad \mathbf{A}_{2,2} = \mathbf{L}_{2,2} \mathbf{U}_{2,2} := \begin{bmatrix} \mathbf{L}_{\alpha\alpha} & & \\ & \mathbf{L}_{\beta,\beta} & \\ \mathbf{L}_{\gamma,\alpha} & \mathbf{L}_{\gamma,\beta} & \mathbf{L}_{\gamma,\gamma} \end{bmatrix} \begin{bmatrix} \mathbf{U}_{\alpha,\alpha} & & \mathbf{U}_{\alpha,\gamma} \\ & \mathbf{U}_{\beta,\beta} & \mathbf{U}_{\beta,\gamma} \\ & & \mathbf{U}_{\gamma,\gamma} \end{bmatrix}$$

The formula for $(\mathbf{T}_{1,1})_{F,B}$ can be re-written as

$$(34) \quad (\mathbf{T}_{1,1})_{F,B} = \mathbf{A}_{F,B} - \left(\mathbf{A}_{F,2} \mathbf{U}_{2,2}^{-1} \right) \left(\mathbf{L}_{2,2}^{-1} \mathbf{A}_{2,B} \right) := \mathbf{A}_{F,B} - \mathbf{X}_{F,2} \mathbf{Y}_{2,B}$$

The factors $\mathbf{X}_{F,2}$ and $\mathbf{Y}_{2,B}$ have sparse structure, due the sparsity in the factorization (33) and the sparsity of $\mathbf{A}_{F,2}$ and $\mathbf{A}_{2,B}$.

$$(35) \quad \mathbf{X}_{F,2} = \begin{bmatrix} \mathbf{A}_{F,\alpha} & \mathbf{0} & \mathbf{A}_{F,\gamma} \end{bmatrix} \mathbf{U}_{22}^{-1}, \quad \mathbf{Y}_{2,B} = \mathbf{L}_{22}^{-1} \begin{bmatrix} \mathbf{0} \\ \mathbf{A}_{\beta,B} \\ \mathbf{A}_{\gamma,B} \end{bmatrix}$$

The factors $\mathbf{X}_{F,2}$ and $\mathbf{Y}_{2,B}$ have the same sparsity pattern as $\mathbf{A}_{F,2}$ and $\mathbf{A}_{2,B}$, respectively. As a result,

$$(36) \quad (\mathbf{T}_{1,1})_{F,B} = \mathbf{A}_{F,B} - \begin{bmatrix} \mathbf{X}_{F,\alpha} & \mathbf{0} & \mathbf{X}_{F,\gamma} \end{bmatrix} \begin{bmatrix} \mathbf{0} \\ \mathbf{Y}_{\beta,B} \\ \mathbf{Y}_{\gamma,B} \end{bmatrix} = \begin{matrix} \mathbf{A}_{F,B} \\ \text{sparse, } O(1) \text{ entries} \end{matrix} - \begin{matrix} \mathbf{X}_{F,\gamma} \mathbf{Y}_{\gamma,B} \\ \text{exact rank } 2b \end{matrix}.$$

Similar reasoning can be used to show the result for $(\mathbf{T}_{11})_{B,F}$.

REFERENCES

- [1] Ahmad Abdelfattah, Pieter Ghysels, Wajih Boukaram, Stanimire Tomov, Xiaoye Sherry Li, and Jack Dongarra. Addressing irregular patterns of matrix computations on GPUs and their impact on applications powered by sparse direct solvers. In *Proceedings of the International Conference on High Performance Computing, Networking, Storage and Analysis*, pages 1–14, 2022.
- [2] Patrick Amestoy, Alfredo Buttari, Jean-Yves l’Excellent, and Theo Mary. On the complexity of the block low-rank multifrontal factorization. *SIAM Journal on Scientific Computing*, 39(4):A1710–A1740, 2017.
- [3] Patrick R Amestoy, Timothy A Davis, and Iain S Duff. An approximate minimum degree ordering algorithm. *SIAM Journal on Matrix Analysis and Applications*, 17(4):886–905, 1996.
- [4] Tracy Babb, Adrianna Gillman, Sijia Hao, and Per-Gunnar Martinsson. An accelerated Poisson solver based on multidomain spectral discretization. *BIT Numerical Mathematics*, 58:851–879, 2018.
- [5] Mario Bebendorf. *Hierarchical matrices*, volume 63 of *Lecture Notes in Computational Science and Engineering*. Springer-Verlag, Berlin, 2008. A means to efficiently solve elliptic boundary value problems.
- [6] Hadrien Bériot, Albert Prinn, and Gwénaél Gabard. Efficient implementation of high-order finite elements for Helmholtz problems. *International Journal for Numerical Methods in Engineering*, 106(3):213–240, 2016.
- [7] Matthias Bollhöfer, Olaf Schenk, Radim Janalik, Steve Hamm, and Kiran Gullapalli. State-of-the-art sparse direct solvers. In *Parallel Algorithms in Computational Science and Engineering*, pages 3–33. Springer, 2020.
- [8] Wajih Boukaram, George Turkiyyah, and David Keyes. Hierarchical matrix operations on GPUs: Matrix-vector multiplication and compression. *ACM Transactions on Mathematical Software (TOMS)*, 45(1):1–28, 2019.
- [9] Luiz Mariano Carvalho, Luc Giraud, and Patrick Le Tallec. Algebraic two-level preconditioners for the Schur complement method. *SIAM Journal on Scientific Computing*, 22(6):1987–2005, 2001.
- [10] Gustavo Chávez, George Turkiyyah, Stefano Zampini, Hatem Ltaief, and David Keyes. Accelerated cyclic reduction: A distributed-memory fast solver for structured linear systems. *Parallel Computing*, 74:65–83, 2018.
- [11] Chao Chen and Per-Gunnar Martinsson. Solving Linear Systems on a GPU with Hierarchically Off-Diagonal Low-Rank Approximations. *arXiv preprint arXiv:2208.06290*, 2022.
- [12] Timothy A Davis. *Direct methods for sparse linear systems*, volume 2. Siam, 2006.
- [13] Timothy A. Davis, Sivasankaran Rajamanickam, and Wissam M. Sid-Lakhdar. A survey of direct methods for sparse linear systems. *Acta Numerica*, 25:383 – 566, 2016.

- [14] Arnaud Deraemaeker, Ivo Babuška, and Philippe Bouillard. Dispersion and pollution of the FEM solution for the Helmholtz equation in one, two and three dimensions. *International journal for numerical methods in engineering*, 46(4):471–499, 1999.
- [15] I.S. Duff, A.M. Erisman, and J.K. Reid. *Direct Methods for Sparse Matrices*. Oxford, 1989.
- [16] Björn Engquist and Lexing Ying. Sweeping preconditioner for the Helmholtz equation: hierarchical matrix representation. *Communications on pure and applied mathematics*, 64(5):697–735, 2011.
- [17] Oliver G Ernst and Martin J Gander. Why it is difficult to solve Helmholtz problems with classical iterative methods. *Numerical analysis of multiscale problems*, pages 325–363, 2012.
- [18] Martin J Gander and Hui Zhang. Restrictions on the use of sweeping type preconditioners for Helmholtz problems. In *International Conference on Domain Decomposition Methods*, pages 321–332. Springer, 2017.
- [19] A. George. Nested dissection of a regular finite element mesh. *SIAM J. on Numerical Analysis*, 10:345–363, 1973.
- [20] P. Ghysels, X. Li, F. Rouet, S. Williams, and A. Napov. An Efficient Multicore Implementation of a Novel HSS-Structured Multifrontal Solver Using Randomized Sampling. *SIAM Journal on Scientific Computing*, 38(5):S358–S384, 2016.
- [21] Pieter Ghysels and Ryan Synk. High performance sparse multifrontal solvers on modern GPUs. *Parallel Computing*, 110:102897, 2022.
- [22] Adrianna Gillman, AlexH. Barnett, and Per-Gunnar Martinsson. A spectrally accurate direct solution technique for frequency-domain scattering problems with variable media. *BIT Numerical Mathematics*, 55(1):141–170, 2015.
- [23] Adrianna Gillman and Per-Gunnar Martinsson. A direct solver with $O(N)$ complexity for variable coefficient elliptic PDEs discretized via a high-order composite spectral collocation method. *SIAM Journal on Scientific Computing*, 36(4):A2023–A2046, 2014.
- [24] Adrianna Gillman, Patrick Young, and Per-Gunnar Martinsson. A direct solver $o(n)$ complexity for integral equations on one-dimensional domains. *Frontiers of Mathematics in China*, 7:217–247, 2012. 10.1007/s11464-012-0188-3.
- [25] Wolfgang Hackbusch. *Hierarchical matrices: algorithms and analysis*, volume 49. Springer, 2015.
- [26] Sijia Hao and Per-Gunnar Martinsson. A direct solver for elliptic PDEs in three dimensions based on hierarchical merging of Poincaré–Steklov operators. *Journal of Computational and Applied Mathematics*, 308:419–434, 2016.
- [27] James Levitt and Per-Gunnar Martinsson. Linear-Complexity Black-Box Randomized Compression of Hierarchically Block Separable Matrices. *arXiv preprint arXiv:2205.02990*, 2022.
- [28] Xiaoye S Li and Meiyue Shao. A supernodal approach to incomplete LU factorization with partial pivoting. *ACM Transactions on Mathematical Software (TOMS)*, 37(4):1–20, 2011.
- [29] L. Lin, J. Lu, and L. Ying. Fast construction of hierarchical matrix representation from matrix-vector multiplication. *Journal of Computational Physics*, 230(10):4071 – 4087, 2011.
- [30] Per-Gunnar Martinsson. A direct solver for variable coefficient elliptic PDEs discretized via a composite spectral collocation method. *Journal of Computational Physics*, 242:460–479, 2013.
- [31] Per-Gunnar Martinsson. Compressing rank-structured matrices via randomized sampling. *SIAM Journal on Scientific Computing*, 38(4):A1959–A1986, 2016.
- [32] Per-Gunnar Martinsson. *Fast direct solvers for elliptic PDEs*. SIAM, 2019.
- [33] Per-Gunnar Martinsson and Joel A Tropp. Randomized numerical linear algebra: Foundations and algorithms. *Acta Numerica*, 29:403–572, 2020.
- [34] P.G. Martinsson. A fast randomized algorithm for computing a hierarchically semiseparable representation of a matrix. *SIAM Journal on Matrix Analysis and Applications*, 32(4):1251–1274, 2011.
- [35] P.G. Martinsson. A direct solver for variable coefficient elliptic pdes discretized via a composite spectral collocation method. *Journal of Computational Physics*, 242(0):460 – 479, 2013.
- [36] Grégoire Pichon, Eric Darve, Mathieu Faverge, Pierre Ramet, and Jean Roman. Sparse supernodal solver using block low-rank compression. In *2017 IEEE International Parallel and Distributed Processing Symposium Workshops (IPDPSW)*, pages 1138–1147. IEEE, 2017.
- [37] Yousef Saad and Maria Sosonkina. Distributed schur complement techniques for general sparse linear systems. *SIAM Journal on Scientific Computing*, 21(4):1337–1356, 1999.
- [38] Alexandre Vion, R Bélanger-Rioux, L Demanet, and Christophe Geuzaine. A DDM double sweep preconditioner for the Helmholtz equation with matrix probing of the DtN map. *Mathematical and Numerical Aspects of Wave Propagation WAVES*, 2013, 2013.
- [39] Richard Vuduc, Aparna Chandramowlishwaran, Jee Choi, Murat Guney, and Aashay Shringarpure. On the limits of GPU acceleration. In *Proceedings of the 2nd USENIX conference on Hot topics in parallelism*, volume 13, 2010.

- [40] Shen Wang, Xiaoye S Li, Jianlin Xia, Yingchong Situ, and Maarten V De Hoop. Efficient scalable algorithms for solving dense linear systems with hierarchically semiseparable structures. *SIAM Journal on Scientific Computing*, 35(6):C519–C544, 2013.
- [41] J. Xia, S. Chandrasekaran, M. Gu, and X.S. Li. Fast algorithms for hierarchically semiseparable matrices. *Numerical Linear Algebra with Applications*, 17(6):953–976, 2010.
- [42] Jianlin Xia, Shivkumar Chandrasekaran, Ming Gu, and Xiaoye S. Li. Superfast multifrontal method for large structured linear systems of equations. *SIAM J. Matrix Anal. Appl.*, 31(3):1382–1411, 2010.
- [43] Anna Yesypenko and Per-Gunnar Martinsson. GPU optimizations for the Hierarchical Poincaré-Steklov Scheme. *arXiv preprint arXiv:2211.14969*, 2022.